RESEARCH ARTICLE

Teleseismic Detection of a Slow Precursor to the Great 1989 Macquarie Ridge Earthquake

Pierre F. Ihmlé, Paolo Harabaglia, Thomas H. Jordan

Low-frequency spectra for the 1989 Macquarie Ridge earthquake (magnitude 8.2) show an amplitude increase and a phase-delay decrease below 6 millihertz that require a short-term slow precursor. This earthquake can be modeled as a compound event in which a fast-rupturing, ordinary earthquake was initiated by an episode of slow, smooth deformation that began more than 100 seconds before the main shock. The moment released in the slow precursor was large, about 3 × 10^20 newton-meters, equivalent to an event of magnitude 7.6. The data are consistent with the precursor being generated in a region of the oceanic upper mantle below the main rupture.

Slow precursors associated with the nucleation of large earthquakes are interesting because their behavior may be key for understanding the mechanics of the rupture process; in particular, detecting them on strainmeters close to active faults is one strategy for short-term earthquake prediction (*1*). Near-field data with adequate resolution to see such precursors are available in only a few areas, however, so there is considerable motivation to observe them at large (teleseismic) distances. In the far-field, the primary signature of a slow precursor is contained in the low-frequency waves that are preferentially excited by sources with long time constants. Slow precursors have been teleseismically detected in the low-frequency radiation from several major earthquakes, including the great 1960 Chilean earthquake (*2*), the 1970 Colombian and 1963 Peru-Boliva deep-focus earthquakes (*3*), and the 1983 intermediate-focus event on the Peru-Ecuador border (*4*). These events occurred in subduction zones, and all but the Chilean event had foci with depths greater than 100 km. Here we use data collected from the newly installed, high-performance seismic networks to establish the occurrence of a large, short-term, slow precursor to a shallow-focus earthquake in a different tectonic regime: the great 1989 Macquarie Ridge earthquake of 23 May 1989, which was located on a transform fault in oceanic lithosphere south of New Zealand (Fig. 1).

The Macquarie Ridge earthquake had a static moment M_T^0 of about 20 × 10^{20} newton-meters (Nm) and moment-magnitude M_W of 8.2, making it the largest seismic event since 1979 (*5*). It was one of the first great earthquakes to be registered by a large network of broadband, triaxial, digital seismographs with high-dynamic range (Fig. 1). The main shock can be approximated by a simple double-couple mechanism (*6*) dominated by right-lateral movement on a 200-km segment of the boundary between the Australian and Pacific plates. Several groups of investigators (*7–9*) have inverted the broadband wave forms to obtain information about the time dependence of the faulting, which can be specified in terms of a source time (or moment-rate) function $\dot{M}_T(t)$ (Fig. 2A). The models differ substantially, especially in terms of the low-order polynomial moments of $\dot{M}_T(t)$ that describe the source behavior at low frequencies (*10*). Braunmiller and Nabelek (*7*) reported the smallest total static moment M_T^0 and the most compact time function, as measured by the centroid time shift Δt_1 and characteristic duration τ_c. They inverted only the body waves, whereas Ekström and Romanowicz (*8*) and Anderson and Zhang (*9*) constrained their solutions to satisfy the moment determined from low-frequency [3 to 6 millihertz (mHz)] surface waves. The moment discrepancy led Anderson and Zhang to conclude that the main rupture was accompanied by an episode of slow moment release, perhaps in the mantle below the seismogenic zone. Interestingly, the value of M_T^0 derived from the Harvard centroid moment tensor (CMT), which also used surface-wave data (*6*), agrees best with the Braunmiller-Nabelek source time function.

Additional discrepancies are revealed by a comparison of the published source time functions with the low-frequency spectra recovered by the methods outlined below (Fig. 2, B and C). We express the Fourier spectrum of the moment-rate function as

$$\int_{-\infty}^{\infty} \dot{M}_T(t) e^{-i\omega(t-t_0)}\, dt = M_T(\omega) e^{-i\omega\Delta t(\omega)}$$

where ω is the angular frequency, $M_T(\omega) \geq 0$ is the amplitude spectrum, and $\Delta t(\omega)$ is the phase-delay spectrum, defined relative to the origin time t_0 determined from the high-frequency waves (*11*). The Anderson-Zhang model provides a rough fit to our estimates of $M_T(\omega)$, but none of the three models even qualitatively matches the observed shape of $\Delta t(\omega)$. In particular, the phase delays from all three models decrease monotonically, corresponding to a positive skewness in $\dot{M}_T(t)$, whereas the actual data show a distinct increase in the phase delay from 1 to 6 mHz.

This increase is diagnostic of an episode of slow, smooth moment release that began before, and initiated, the main rupture of the Macquarie Ridge earthquake. A

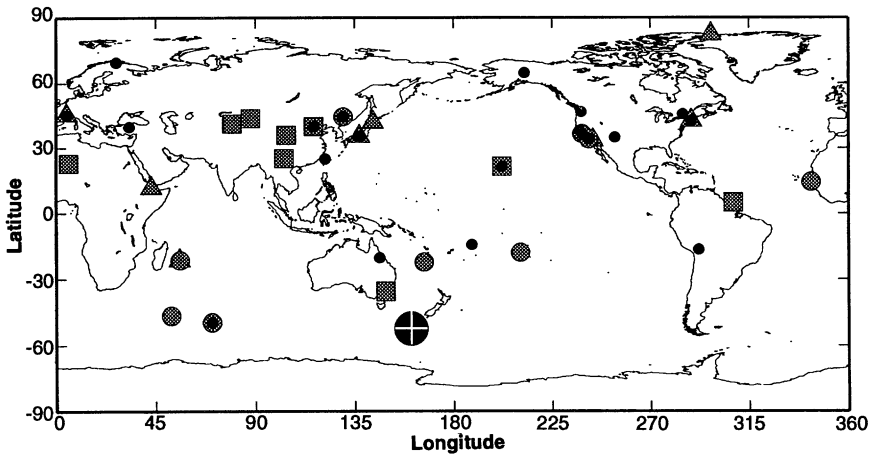

Fig. 1. Map showing location of the 1989 Macquarie Ridge earthquake (white cross) and seismic stations, which include elements of the CDSN, GEOSCOPE, GDSN, IDA, and IRIS networks. Large shaded symbols are stations used in the low-frequency analysis: vertical only, triangles; tranverse only, squares; and both, circles. Small black dots are stations used in the high-frequency *P*-wave analysis.

The authors are in the Department of Earth, Atmospheric, and Planetary Sciences, Massachusetts Institute of Technology, Cambridge, MA 02139.

compound source, comprising a main rupture with a static moment of 16×10^{20} Nm superposed on an episode of slow deformation with a static moment of 6×10^{20} Nm, satisfies the low-frequency spectra (Fig. 3). According to this simple model, over half of the slow deformation occurred in a 130-s interval before the beginning of the main rupture. Hence, if the model's main features are valid, the slow precursor to the Macquarie Ridge earthquake was itself an event of $M_W \approx 7.6$.

Low-frequency observations. We obtained the spectral data in Fig. 2 by two methods having different sensitivities to unmodeled propagation effects. The first was an analysis of normal modes based on spectral integrals computed from 6-hour time series, which include up to fourth-orbit Rayleigh waves (R_4) and fifth-orbit Love waves (G_5). We recovered the total-moment spectrum $M_T(\omega)$ using a variant of the method described by Silver and Jordan (*12*), and we derived the phase-delay spectrum $\Delta t(\omega)$ using an algorithm formulated by Riedesel and Jordan (*13*). Because in the derivation of the phase-delay spectrum we integrated over individual modes, the method was not applied at frequencies above 11 mHz, where the spectrum becomes densely populated and the fundamental-mode resonance peaks begin to overlap considerably.

The second technique was a traveling-wave method based on broadband cross-correlagrams of fundamental-mode mantle waves (*14*). To minimize the effects of aspherical heterogeneities, we processed only the first-orbit groups, R_1 on vertical components and G_1 on transverse components. Spectra similar to those in Fig. 2 were obtained from the second-orbit mantle waves, however, an observation that precludes strong directivity effects.

Both the normal-mode and traveling-wave techniques rely on synthetic seismograms to model the source geometry and propagation effects. We calculated all synthetics by normal-mode summation using the spherically symmetric, nonrotating, anisotropic, anelastic structure of PREM (*15*) and the aspherical, elastic structure of SH8/WM13. The latter is a tomographic model derived by Woodward *et al.* (*16*) from the inversion of wave form and travel-time data out to spherical-harmonic degree and order eight. Aspherical corrections to the eigenfrequencies and eigenfunctions were based on the asymptotic theory of Woodhouse and Dziewonski (*17*).

We culled and edited the available long-period seismograms (*18*), obtaining 18 vertical and 18 transverse components from 27 stations with good global distribution (Fig. 1). These were inverted for the moment-tensor spectrum and centroid depth. The maximum reduction of variance was obtained for a centroid depth of 23 km, 8 km deeper than the CMT value; shallower centroids yielded a poorer fit in the lower frequency bands (1 to 3 mHz), whereas deeper centroids gave a poor fit at high frequencies (>7 mHz). We also varied the geographical location of the centroid; the spectra were insensitive to these parameters. The high-frequency values in the spectrum of mechanism tensors, $\hat{\mathbf{M}}(\omega)$ (Fig. 4), are consistent with the Harvard CMT, but below 6 mHz the mechanism shows a rotation of up to ~35° about the principal compressional (P) axis. This rotation may indicate that the slow component had a different mechanism than the main rupture. However, the rotation is almost entirely a result of variations in the $M_{r\theta}$ and $M_{r\varphi}$ components, which tend to be poorly constrained at low frequencies for shallow-focus events (*19*). Because of this uncertainty, the spectral estimation in Fig. 2 was done with synthetic seismograms calculated for a point source with the frequency-independent CMT mechanism. Inversions with the frequency-dependent mechanisms of Fig. 4 gave essentially identical results.

Assessment of propagation bias. There are several independent checks on the efficacy of the spectra-recovery procedures in eliminating propagation effects. First, the spectra derived by the standing-wave and traveling-wave algorithms are in excellent agreement, despite the differing sensitivities of the two methodologies to various types of scattered signals. The modal techniques rely on temporal and spectral averaging to reduce scattering effects, whereas the traveling-wave method captures information about the source from the first-orbit surface waves, which have not had much time to interact with aspherical heterogeneities.

We performed separate inversions of the vertically and transversely polarized data sets, obtaining the four spectra in Fig. 5. The torodial-mode (*T*) and Love-wave (*L*) spectra derived from the transverse components are systematically lower than the vertical-component spheroidal-mode (*S*) and Rayleigh-wave (*R*) spectra at frequencies above 10 mHz, perhaps because the spherically symmetric PREM attenuation model inadequately represents the anelastic structure of the upper mantle along the paths sampled in this experiment (*20*). The

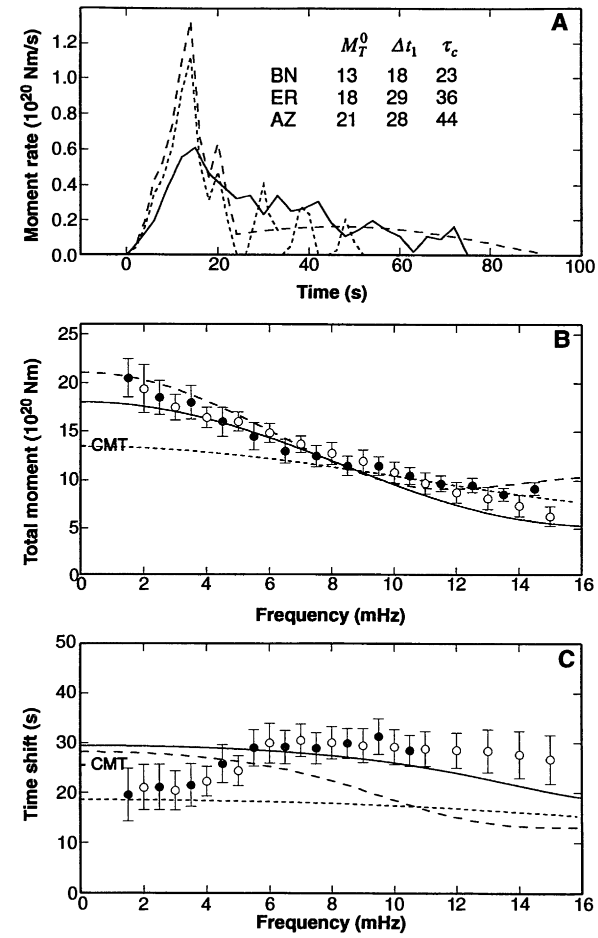

Fig. 2. (**A**) Three source time functions $M_T(t)$ for the Macquarie Ridge earthquake obtained from broadband wave form inversions by Braunmiller and Nabelek (*7*) (BN, short dashed line), Ekström and Romanowicz (*8*) (ER, solid line), and Anderson and Zhang (*9*) (AZ, long dashed line). Table gives M_T^0 (in units of 10^{20} Nm), Δt_1, and τ_c (both in seconds) for the three source time functions. (**B**) Amplitude and (**C**) phase-delay spectra for this earthquake, defined according to the conventions of (*4*). The phase-delay spectrum is referenced to the NEIC origin time (*11*). Harvard CMT values of M_T^0 and Δt_1 (*6*) are indicated as zero-frequency intercepts. The three lines are the spectra computed by Fourier transforming the source time functions in (A). Points with standard deviations are the low-frequency data obtained in this study. Results from two separate methods are shown: Standing-wave analysis using 6-hour records (solid circles) and traveling-wave analysis using only the R_1 and G_1 wave groups (open circles). Because of mode overlap, phase-delays were not measured by the normal-mode method above 11 mHz. The two methods have different sensitivities to unmodeled propagation effects; therefore, the good agreement indicates that the propagation bias is likely to be small.

standing-wave ($S + T$) and traveling-wave ($R + L$) averages at these frequencies are in good agreement with the source models derived from broadband wave form analysis, however (Fig. 2B). All four spectra show a decrease in the phase delay below 6 mHz, which is the primary signature of the slow precursor, although this feature is more strongly expressed in the vertical-component estimates. This difference would be expected if the slow precursor had a mechanism with more of a dip-slip component than the main rupture, a hypothesis consistent with the frequency dependence in Fig. 4. In any case, the general agreement shown among the four types of spectra makes it unlikely that unmodeled propagation effects can explain the basic features of the spectra in Fig. 3.

As a further check, we generated synthetic seismograms for the data set using a non-asymptotic code that incorporates along-branch aspherical coupling among the fundamental modes and Coriolis coupling between fundamental spheroidal and toroidal modes (*21*). Experiments with these synthetics demonstrate that these types of mode coupling have a negligible effect on the spectra recovered by the normal-mode analysis. Evidently, the spectral averaging used in the modal techniques, combined with the criteria used to select the data, are effective in eliminating any coupling bias.

Because the 12- to 16-km-thick oceanic crust in the focal zone (*9*) is different from the PREM structure, we investigated the excitation anomalies attributed to near-source structure by computing synthetic seismograms based on an adiabatic mode approximation (*22*). Again, the effects were found to be inconsequential.

The teleseismic techniques have also been validated by applying them to a variety of earthquakes studied by other methods. For example, the spectra recovered for the 1992 Landers earthquake ($M_W = 7.3$), the 1989 Loma Prieta earthquake ($M_W = 6.9$), and other large strike-slip California events are consistent with the source mechanisms and moment-rate functions determined from near-field data, which preclude these events from having slow precursors observable at teleseismic distances (*23*). Moreover, the amplitude and phase-delay spectra derived by these same techniques for high-stress-drop, deep-focus events are observed to be flat, as expected for sources with compact time functions, and to have static moments and centroid time shifts in good agreement with the Harvard CMT values.

Evidence for a slow precursor. The source time function in Fig. 3 is not unique in providing a good fit to the low-frequency spectra, but theoretical arguments and numerical experiments confirm that all models that fit these data do have a slow precursor. Assuming that the source time function is nonnegative (no-backslip) and the mechanism is constant, Jordan (*4*) derived a set of inequalities among low-order polynomial moments of $\dot{M}_T(t)$ and used them to detect a slow precursor for the 26 April 1983 Peru-Ecuador intermediate-focus earthquake. We can apply one of Jordan's inequalities to show that the upward curvature of the phase-delay spectrum at low frequencies requires a slow precursor—that is, the start time t_* must have been less than the high-

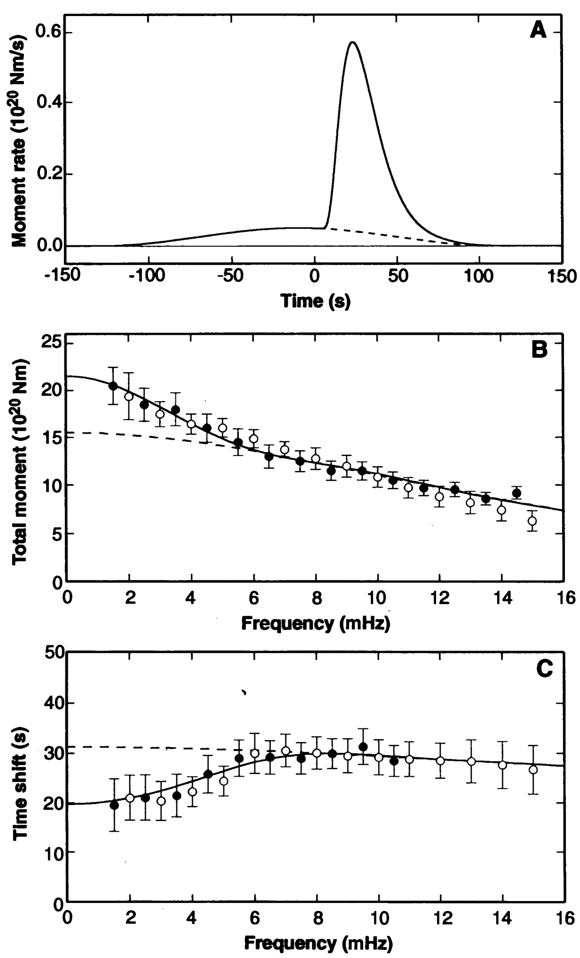

Fig. 3. (**A**) A simple, compound-source model of $\dot{M}_T(t)$ for the 1989 Macquarie Ridge earthquake that fits the low-frequency observations. The earthquake began with a slow event, here represented by a symmetric Hanning function (cosine-square bell) with a moment of 6×10^{20} Nm and a total duration of 240 s, starting 130 s before the high-frequency origin time ($t = 0$). The main (fast) event is represented by a function of the form $Ae^{-a/t - t/b}H(t)$, where $a = 55$ s, $b = 10$ s, H is the Heaviside step function, and the constant A is chosen to give a static moment of 16×10^{20} Nm. The dashed line indicates the contribution of the slow component for $t > 0$. (**B**) Amplitude and (**C**) phase-delay spectra, comparing this model (solid lines) with the data from Fig. 2 (circles). The dashed lines are the spectra of the main event alone, which show that the signature of the slow component is confined to frequencies less than 6 mHz.

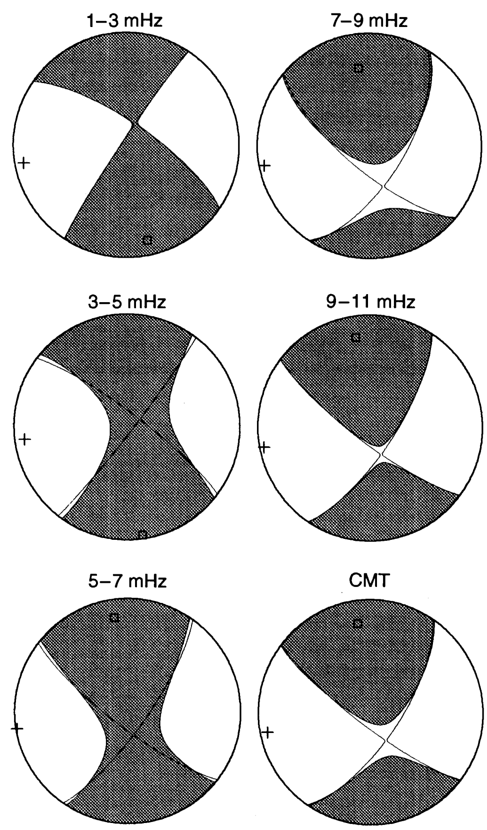

Fig. 4. Lower focal hemisphere projections of the source mechanism for the 1989 Macquarie Ridge earthquake. The first five diagrams are estimates obtained from spheroidal and toroidal mode data in 2-mHz bands using the inversion algorithm of Riedesel and Jordan (*13*); the sixth is the Harvard CMT solution (*6*). The compressional (P) and tensional (T) axes are indicated with a cross and an open square, respectively. The shaded region is the compressional field of *P*-wave radiation and the thin solid lines indicate the nodal planes of the best-fitting double couple. A systematic rotation of the mechanism about the P axis is observed at the lower frequencies, indicating that the slow precursor may have had a significant dip-slip component.

frequency origin time t_0—without appealing to a specific source time function (*24*).

We also tested for the requirement of a slow precursor by direct inversion of the spectral data under the no-backslip, constant-mechanism assumption. The phase and amplitude data were combined to form estimates of the complex Fourier spectrum, which yields a set of linear constraints on $\dot{M}_T(t)$. We inverted the spectral estimates for $\dot{M}_T(t)$ discretized at a 1-s sampling rate using a quadratic programming algorithm (*25*). Smoothness constraints were imposed on $\dot{M}_T(t)$ before t_0, and the start times t_* were varied from t_0 to $t_0 - 400$ s. For all values of t_* within 100 s of t_0, solutions could not be found that provided acceptable fits to the data, even when the smoothness constraints were relaxed, consistent with the hypothesis test based on Jordan's inequality. Inversions with $t_* = t_0 - 130$ s and heavy smoothing for $t < t_0$ yielded solutions similar to the analytical model in Fig. 3.

Constraints from P waves. The broadband seismograms were examined for a precursor arriving in front of the *P* waves from the main shock, but no signal was observed, even at relatively close, high-gain stations like Nouméa, New Caledonia (NOU), and Charters Towers, Australia (CTAO), where the *P*-wave amplitudes are 800 and 300 times greater than the noise level, respectively (Fig. 6). The absence of such signals places a strong observational constraint on smoothness of the source time function before t_0. Synthetic seismograms computed for the source model in Fig. 3, for example, display a *P*-wave precursor large enough to be easily detected on the time series.

The *P* waves also constrain the source spectrum at higher frequencies. We analyzed *P* wave groups from 21 stations (Fig. 1) using the cross-correlation method (*14*) to obtain amplitude and phase-delay spectra at 2-mHz intervals over a band from 17 to 45 mHz. The phase-delay measurements of the *P* waves are consistent with the surface-wave data to within the standard errors of the two techniques (Fig. 7C). The *P*-wave amplitudes are somewhat higher, in better agreement with the free-oscillation estimates (Fig. 7B).

We inverted the complete data set subject to the requirement that the signal amplitude before the high-frequency *P*-wave arrival time is smaller than the noise levels at NOU and CTAO, which are the stations in our data set with the highest sensitivity to signals from the Macquarie Ridge area. Taking $t_* = t_0 - 400$ s, we obtain the $\dot{M}_T(t)$ plotted in Fig. 7A. The integrated moment of the precursor is 4.7×10^{20} Nm, larger than the one in Fig. 3A; it extends to earlier times and is much smoother. The net effect is to double the perturbation to the phase-delay spectrum at low frequencies (Δt_1 decreases from 20 to 8 s) and increase τ_c from 64 to 116 s. This inversion does not match the phase delays at frequencies less than 5 mHz as well as the previous model does, although the overall fit to the spectral data is quite satisfactory. Moreover, because the time function is smooth for $t < t_0$, it generates a *P*-wave precursory signal that is below the detection threshold at CTAO (Fig. 6), as well as the other stations for which we have seismograms.

The main earthquake is characterized by a large, 20-s episode of moment release beginning 10 s after the high-frequency origin time, followed by a sequence of several smaller subevents ending abruptly at +75 s. The structure for $t > +30$ s is similar to source time function of Ekström and Romanowicz (*8*), although the ability of our data (and theirs) to resolve such details

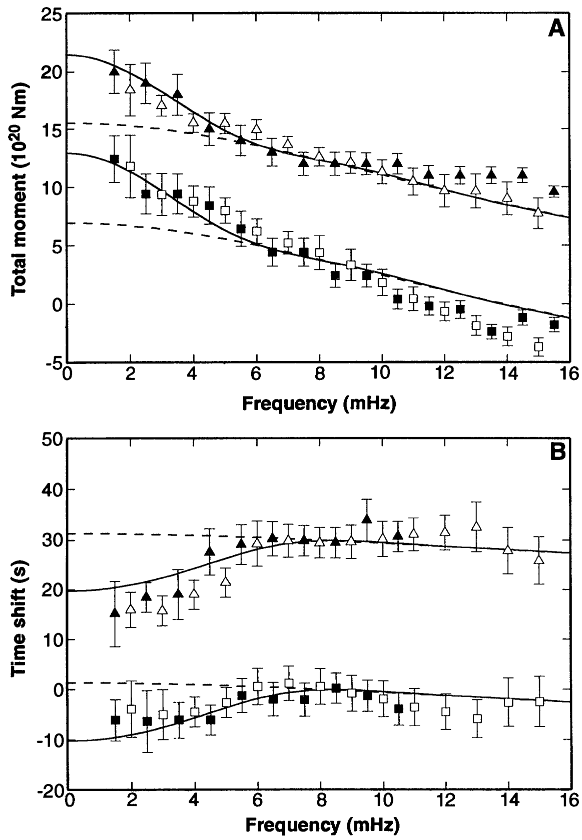

Fig. 5. (**A**) Amplitude and (**B**) phase-delay spectra derived from four different wave types: Spheroidal modes (closed triangles) and first-orbit Rayleigh waves (open triangles) from vertical-component seismograms, and toroidal modes (closed squares) and first-orbit Love waves (open squares) from transverse-component seismograms. For plotting clarity, the transverse-component data have been shifted downward by 9 units in (A) and 30 units in (B). The lines are the same reference spectra, calculated from the model in Fig. 3. All four data types show similar deviations from the main-shock spectrum (dashed lines) below 6 mHz.

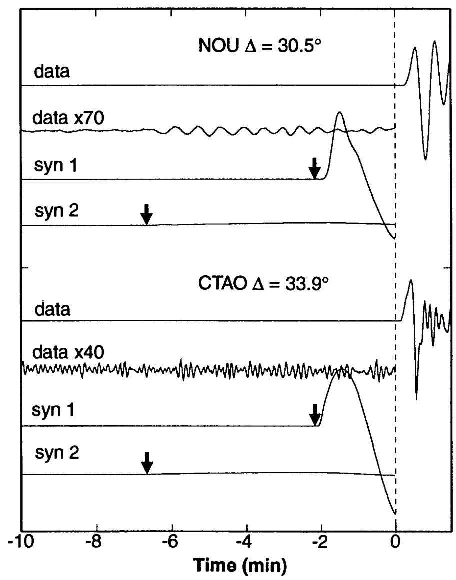

Fig. 6. Comparisons of data and synthetics in 10-min intervals before the *P* waves at GEOSCOPE station NOU (Nouméa, New Caledonia) and GSDN station CTAO (Charters Tower, Australia). Horizontal scale is in minutes, referenced to the high-frequency *P*-wave arrival time (vertical dashed line). First trace in each set is the unfiltered observed seismogram from the long-period vertical channel, arbitrarily normalized to the peak-to-peak amplitude of the *P* wave. Positive time shifts of the first arrivals are primarily due to the group delay of the instrument. The other three traces are amplified by factors of 70 for NOU and 40 for CTAO. The second in each group is again the unfiltered data, showing that no precursor is observed above the noise levels. The third (syn 1) is the ray-theoretical synthetic computed for the analytical source model in Fig. 3A, and the fourth (syn 2) is for the inversion model in Fig. 7A: arrows give the ray-theoretical arrival times for the precursor onsets at $t_0 - 130$ s and $t_0 - 400$ s, respectively. The precursor amplitude for syn 1 is significant above the noise levels, but the amplitude for syn 2 is not.

is questionable. As can be seen from Fig. 7, however, the spectral data require a larger peak amplitude and a significant delay of the main episode relative to their model. (Examination of the short-period seismograms suggests that the 10-s gap between t_0 and the main episode is caused by high-frequency radiation from small subevents.) Our model provides a better fit to both the amplitudes and arrival times of the long-period *P* waves (Fig. 8). Comparisons of transversely polarized *S* waves, which were not used in the spectral estimation, yield similar results.

In summary, the source time function in Fig. 7 satisfies the spectral data from 1 to 45 mHz and is consistent with the time-domain records of the principal body waves, including the lack of any *P*-wave precursor on seismograms from regional high-gain stations. Despite the disappointing absence of any direct observation of a precursor on the time series, we have been unable to erect a viable alternative explanation for the low-frequency data.

Interpretation. The Macquarie Ridge earthquake occurred on an oceanic transform fault. Slow earthquakes—events with anomalously large characteristic durations relative to their static moment—are common on such strike-slip faults (*26*). Our analysis of low-frequency spectra indicates that some slow earthquakes may be initiated by slow precursors (*28*). In continental regions like California and Japan, in contrast, slow earthquakes are infrequent (*29*), and any preseismic nucleation events are constrained by sensitive near-field and regional sensors to be small (*23*). We suspect, therefore, that the existence of slow precursors reflects a stratification in the mechanical properties of the oceanic lithosphere.

The teleseismic data can be satisfied by modeling the Macquarie Ridge earthquake as a compound source comprising two distinct types of faulting. The initial episode was an infraseismic source or quiet earthquake (*30*), radiating significant energy only at the very low end of the seismic spectrum ($\leq$6 mHz). In the inversion model of Fig. 7A, this precursor has a moment-release time function that grows smoothly—approximately exponentially with a time constant of ~100 s—and integrates to a total moment of about 5×10^{20} Nm. The lack of a detectable signal before the main *P*-wave arrivals constrains the high-frequency roll off of its spectrum to decay as ω^{-n} where $n > 3$. We infer that during this transient deformation the rupture velocity v_r and particle velocity $\Delta\dot{u}$ were anomalously low, although the stress drop $\Delta\sigma$ was not; these conditions imply that the rise time for the motion was long (*32*).

Although the location of the slow precursor relative to the Macquarie Ridge main shock is not directly constrained by our data, the variance reduction at frequencies below 3 mHz increases for centroid depths greater than our reference value of 23 km, consistent with other long-period studies (*8, 9*), whereas the variance reduction at higher frequencies decreases. This observa-

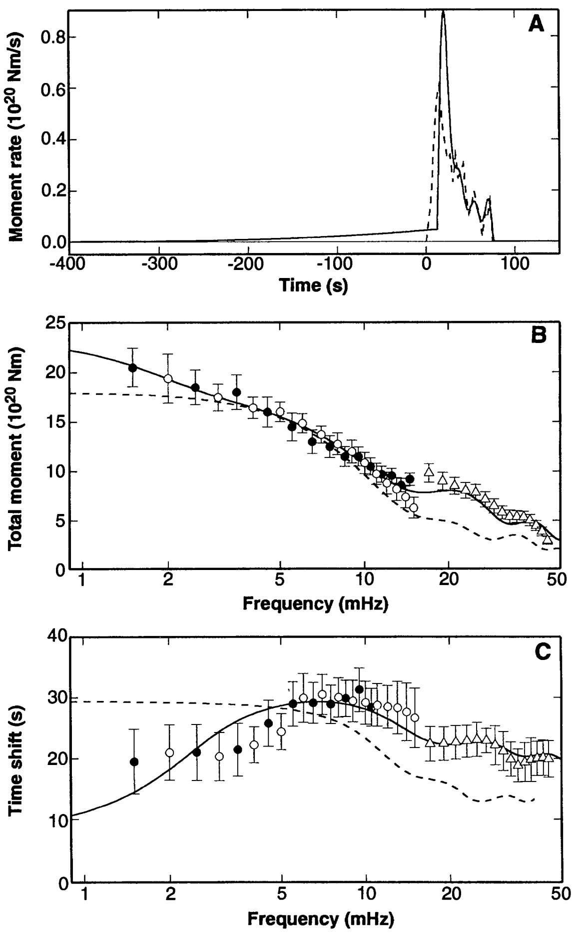

Fig. 7. (**A**) Source time function (solid line) obtained from the inversion of the amplitude and phase-delay spectra in (**B**) and (**C**), compared with the Ekström-Romanowicz (*8*) estimate (dashed line) derived from broadband body waves. The minimization to obtain the former included a smoothing constraint designed to minimize the precursor amplitude on the *P*-wave seismograms in Fig. 6. Data in (B) and (C) are from the analysis of normal modes (solid circles), surface waves (open circles), and *P* waves (open triangles). Solid lines are the spectra predicted by this model; dashed lines are the predictions of the Ekström-Romanowicz model. Time scales are linear with zero at the high-frequency origin time. Frequency scales are logarithmic.

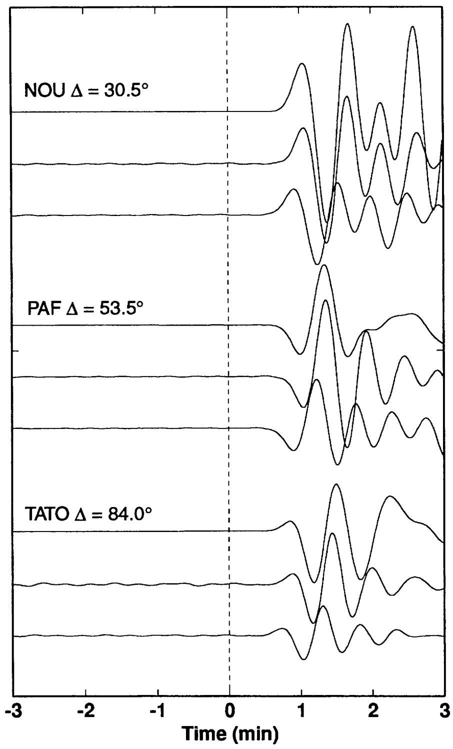

Fig. 8. Comparisons of observed and synthetic *P* waves for vertical-component instruments at Nouméa, New Caledonia (NOU), Port aux Français, Kerguélen Island (PAF), and Taipei, China (TATO). Top trace of each station group is the observed seismogram; middle trace was calculated from the inversion model of Fig. 7A by complete summation of spheroidal modes to 50 mHz; bottom trace was calculated from the Ekström-Romanowicz model (*8*) by the same procedure. The synthetics were based on a PREM structure (*15*), the Harvard CMT centroid and mechanism (*6*), and instrument responses assigned by the network operators. Horizontal scale is in minutes, referenced to the high-frequency *P*-wave arrival time (vertical dashed line). Vertical scale is arbitrary digital units, but the amplitudes of the synthetics relative to the data have been maintained for each station. All seismograms have been low-passed by a 10-pole Butterworth filter with corner at 35 mHz. The shift of the *P*-wave first motion to positive times is a signal delay resulting primarily from the instrument and filter responses. The small ripple in advance of the *P* wave on the synthetics is an artifact of the synthesis procedure. The synthetics for our model provide a better match to the *P*-wave amplitudes and group arrival times on these and most other stations.

tion supports the notion that the quiet earthquake was generated in a region of the oceanic upper mantle below the main episode of faulting.

One plausible explanation for the low values of v_r and $\Delta\dot{u}$ inferred for the quiet earthquake is that the material in this layer undergoes a rapid transition from velocity weakening to velocity strengthening when slip velocities exceed a relatively low threshold value. This behavior is qualitatively consistent with some laboratory experiments on halite (*33*) and granite (*34*), at least at low normal stress (*35*), although the available data indicate that serpentinized peridotites, which are presumably major constituents of the uppermost mantle in the region of the Macquarie earthquake, behave in the opposite sense; that is, they are velocity strengthening at low velocities and velocity weakening at higher velocities (*36*). Slow events would not be expected to nucleate in such a material. The temperature, pressure, and compositional dependence of the transitions from velocity weakening to velocity strengthening are not well understood, however, and more laboratory data are needed.

The moment-tensor inversions displayed in Fig. 4 suggest that the mechanism of the slow precursor may have had a significant dip-slip component. Accounting for such a component increases the estimated size of the precursor. Such a mechanism could help to explain the anomalous excitation of radial free oscillations observed by Park (*37*) and other low-frequency modes observed by Kedar and Tanimoto (*38*).

REFERENCES AND NOTES

1. J. H. Dieterich, *J. Geophys. Res.* **83**, 3940 (1978); J. R. Rice, *Gerlands Beitr. Geophys.* **88**, 91 (1979); T. E. Tullis, *Pure Appl. Geophys.* **126**, 555 (1988).
2. H. Kanamori and J. Cipar, *Phys. Earth Planet. Inter.* **9**, 128 (1974); I. L. Cifuentes and P. G. Silver, *J. Geophys. Res.* **94**, 643 (1989).
3. A. M. Dziewonski and F. Gilbert, *Nature* **247**, 185 (1974).
4. T. H. Jordan, *Geophys. Res. Lett.* **18**, 2019 (1991).
5. A detailed description of the earthquake and its tectonic setting is given in L. J. Ruff, Ed. [*ibid.* **17**, 989 (1990)] and S. Das [*Nature* **357**, 150 (1992)].
6. A. M. Dziewonski, G. Ekstrom, J. H. Woodhouse, G. Zwart, *Phys. Earth Planet. Inter.* **60**, 243 (1990).
7. J. Braunmiller and J. Nabelek, *Geophys. Res. Lett.* **17**, 1017 (1990).
8. G. Ekstrom and B. Romanowicz, *ibid.*, p. 993.
9. H. J. Anderson and J. Zhang, *J. Geophys. Res.* **96**, 19853 (1991).
10. We use Jordan's (*4*) notation and conventions in defining source parameters.
11. We adopt the National Earthquake Information Center value of t_0 = 10:54:46.3 s. Both the amplitude and phase-delay spectra are even functions of frequency (*4*).
12. P. G. Silver and T. H. Jordan, *Geophys. J. R. Astron. Soc.* **70**, 755 (1982); *J. Geophys. Res.* **88**, 3273 (1983). The squared-amplitude spectrum for each seismogram was integrated over 1-mHz bands, and the integrals for all seismograms were inverted with an algorithm optimized to account for aspherical heterogeneity, errors in the assumed source mechanism, and ambient seismic noise.
13. M. A. Riedesel, T. H. Jordan, A. F. Sheehan, P. G. Silver, *Geophys. Res. Lett.* **13**, 609 (1986); M. A. Riedesel and T. H. Jordan, *Bull. Seismol. Soc. Am.* **79**, 85 (1989); see also (*4*). The complex Fourier spectrum for each observed and synthetic seismogram was integrated over narrow (~0.1 mHz) intervals centered on the average eigenfrequencies of the fundamental modes, and we calculated a phase-delay time relative to the synthetic from the peak of a cross-correlation function constructed by summing products of the complex-valued spectral integrals over 1-mHz bands; we then obtained $\Delta t(\omega)$ by averaging the phase-delay times over the network.
14. A. M. Dziewonski, J. Mills, S. Bloch, *Bull. Seismol. Soc. Am.* **62**, 129 (1972); E. Herrin and T. Goforth, *ibid.* **67**, 1259 (1977). The particular procedures are discussed in detail by L. S. Gee and T. H. Jordan, *Geophys. J. Int.* **111**, 363 (1992). We constructed an isolation filter for the target wave group by windowing a synthetic seismogram; it was cross-correlated with the observed seismogram and the complete synthetic, and the cross-correlagrams were windowed in the time domain and narrow-band filtered. The resulting waveforms were fit by five-parameter Gaussian wavelets to obtain relative amplitude and phase delays. Estimates of $M_T(\omega)$ and $\Delta t(\omega)$were then constructed by averaging these residuals over the global network.
15. A. M. Dziewonski and D. L. Anderson, *Phys. Earth Planet. Inter.* **25**, 297 (1981).
16. R. L. Woodward, A. M. Forte, W. Su, A. M. Dziewonski, *J. Geophys. Res.*, in press.
17. J. H. Woodhouse and A. M. Dziewonski, *ibid.* **89**, 5953 (1984).
18. We edited all available seismograms from the IDA, GEOSCOPE, CDSN, and IRIS stations and rotated the horizontals, if available, to obtain the transversely polarized components. We compared the observed records with synthetic seismograms calculated for the CMT source model and rejected those with egregious timing or amplitude problems, large data gaps, or poor signal-to-noise ratios. We then inverted 6-hour records of the selected seismograms for the complete moment-tensor spectrum using the mode-integration algorithm (*13*) and the Harvard CMT centroid depth of 15 km, deriving estimates at 1-mHz intervals from 1.5 to 10.5 mHz. At this stage, seismograms exhibiting poor variance reduction or evidence of significant toroidal-spheroidal cross-coupling were removed. The latter were recognized by quasi-Love waves on the vertical components or quasi-Rayleigh waves on the transverse components. In most cases the coupling was attributed to Coriolis effects, which are strongest for nearly polar paths and for nodal positions in the surface-wave radiation patterns; see J. Park, *J. Geophys. Res.* **91**, 6441 (1986).
19. A. M. Dziewonski, T.-A. Chou, J. H. Woodhouse, *ibid.* **86**, 2852 (1981); H. Kanamori and J. Given, *Phys. Earth Planet. Inter.* **27**, 8 (1981); A. M. Dziewonski and J. H. Woodhouse, *J. Geophys. Res.* **88**, 3247 (1983).
20. In an analysis of a global distribution of earthquakes, we found that the PREM attenuation structure (*15*) is superior to the recently published model of R. Widmer, G. Masters, and F. Gilbert [*Geophys. J. Int.* **104**, 541 (1991)], which predicts quality factors for the 10-mHz fundamental spheroidal modes that are higher by about 10%.
21. The code for computing the coupled-mode synthetics was written by J. Park and modified by P. Puster, based on the first-order subspace projection approximation of J. Park [*Geophys. J. R. Astron. Soc.* **90**, 129 (1987)] and F. A. Dahlen, [*ibid.* **91**, 241 (1987)].
22. A. Levshin, *Ann. Geophys.* **3**, 511 (1985).
23. M. J. S. Johnston, A. T. Linde, M. T. Gladwin, *Geophys. Res. Lett.* **17**, 1777 (1990); S. Takemoto, *J. Geophys. Res.* **96**, 10377 (1991).
24. Jordan's (*4*) inequality (1a) states that any non-negative function $\dot{M}_T(t)$ constrained to be zero before $t = 0$ satisfies $\alpha \equiv \hat{\mu}_3/2\mu_1 \geq -1/8$, where μ_1 is the first moment and $\hat{\mu}_3$ is the third central moment of $\dot{M}_T(t)$. This inequality places an upper bound on the magnitude of the upward curvature of the phase-delay spectrum at zero frequency: $[d^2\Delta t(\omega)/d\omega^2]_{\omega=0} \leq \Delta t_1{}^3/12$. A curvature exceeding this bound is indicative of a moment-release starting time t_* that is less than the high-frequency origin time t_0, which is Jordan's definition of a slow precursor. Because $\Delta t(\omega)$ is an even function of frequency, its slope at the frequency origin is zero, and its behavior for small frequencies can be approximated by the theoretical phase-delay spectrum (*4*), $\Delta t(\omega) = (1 - \alpha)\Delta t_1 + (\alpha/\omega)\arctan \omega\Delta t_1$. To test the null hypothesis that $t_* = t_0$ (no precursor), we computed the misfit of this spectrum to the data in the frequency interval 1 to 6 mHz as a function of Δt_1 and α. Using Jordan's inequality, we could reject the null hypothesis in favor of the alternative (the Macquarie Ridge earthquake had a slow precursor) at the 95% confidence level.
25. The algorithm minimizes a linear combination of a chi-square measure of spectral misfit and a quadratic form measuring the roughness of $\dot{M}_T(t)$, subject to the constraints that $\dot{M}_T(t) \geq 0$ for $t \in [t_*, t_{max}]$ and $\dot{M}_T(t) = 0$ for $t \notin [t_*, t_{max}]$. The computer code, written by R. L. Parker and P. Stark, was adapted from C. L. Lawson and R. J. Hanson [*Solving Least Squares Problems* (Prentice-Hall, Englewood Cliffs, NJ, 1974), pp. 160–165].
26. H. Kanamori and G. S. Stewart, *Phys. Earth Planet. Int.* **11**, 312 (1976); *ibid.* **18**, 167 (1979); E. A. Okal and L. M. Stewart, *Earth Planet. Sci. Lett.* **57**, 75 (1982); A. G. Prozorov and F. J. Sabina, *Geophys. J. R. Astron. Soc.* **76**, 317 (1984). In a systematic survey of anomalous free-oscillation excitations during the 2-year period 1978 to 1979, Beroza and Jordan (*27*) identified 14 slow earthquakes with $M_W \geq 6.2$; all were in oceanic lithosphere and 11 were on oceanic transform faults.
27. G. C. Beroza and T. H. Jordan, *J. Geophys. Res.* **95**, 2485 (1990).
28. Using data from the IDA network, we derived values of M_T^0, τ_c, Δt_1, and α from low-frequency source spectra for a global population of earthquakes from 1978 to 1989 and tested for the existence of slow precursors using the inequalities derived in (*4*); among 20 oceanic transform earthquakes with $M_W \geq 6.5$; the hypothesis that $t_* = t_0$ could be rejected in favor of the alternative, $t_* < t_0$, for approximately half [T. H. Jordan, P. F. Ihmlé, P. Harabaglia, *Eos* **72**, 201 (1991)].
29. A few small, slow events have been detected by strainmeters in Japan (*31*) and California [H. Kanamori, *Geophys. Res. Lett.* **16**, 1411 (1989)].
30. The term infraseismic was used by Sacks *et al.* (*31*) in their seminal paper on slow and silent earthquakes detected by strainmeters. Infraseismic sources were postulated by Beroza and Jordan (*27*) to explain anomalous episodes of low-frequency normal-mode excitation detected by the IDA network during periods when no ordinary earthquakes were observed. We have adopted the term "quiet earthquake" to describe an infraseismic event that excites free oscillations but does not produce detectable wave groups on seismograms at teleseismic distances (*4*).
31. I. S. Sacks, S. Suyehiro, A. T. Linde, J. A. Snoke, *Nature* **275**, 599 (1978).
32. The characteristic velocity of the source process is $v_c = L_c/\tau_c$, where L_c is a characteristic dimension. For the main event, $\tau_c \approx 33$ s. If L_c for the precursor is the same or smaller than for the main event, then $\tau_c > 100$ s for the former implies that v_c was at least three times less (the precursor was slow). Since the static moment of the slow component was a significant fraction of the entire event, the average fault displacement Δu and stress drop $\Delta\sigma$ of the precursor were comparable to those of the main event. The conclusion that v_r and $\Delta\dot{u}$ are anomalously small follows from the scaling relations, $v_c \sim (v_r^2\,\Delta\dot{u})^{1/3}$ and $\Delta\sigma \approx \mu\Delta\dot{u}/v_r$,

valid for an ω^{-3} model [F. A. Dahlen, *Bull. Seismol. Soc. Am.* **64**, 1159 (1974); K. Aki and P. G. Richards, *Quantitative Seismology* (Freeman, San Francisco, 1980), vol. 2, chap. 14]. A small value of $\Delta \dot{u}$ implies that the rise time of the slow precursor must be anomalously long.
33. T. Shimamoto and J. Logan, in *Earthquake Source Mechanics*, S. Das, J. Boatwright, C. Scholz, Eds., vol. 37 of *Geophysical Monographs* (American Geophysical Union, Washington, DC, 1986), pp. 49–63.
34. M. L. Blanpied, T. E. Tullis, J. D. Weeks, *Geophys. Res. Lett.* **14**, 554 (1987).
35. B. D. Kilgore, M. L. Banpied, J. H. Dieterich, *ibid.*, in press.
36. L. A. Reinen, J. D. Weeks, T. E. Tullis, *ibid.* **18**, 1921 (1991); L. A. Reinen, T. E. Tullis, J. D. Weeks, *ibid.* **19**, 1535 (1992).
37. J. Park, *ibid.* **17**, 1005 (1990). Park observed radial mode with amplitudes significantly higher than expected for a pure strike-slip mechanism; he found that although the radial overtones ${}_1S_0$ to ${}_5S_0$ could plausibly be explained by mode coupling, the fundamental mode ${}_0S_0$ could not. He therefore postulated the existence of a dip-slip or isotropic component with a moment of $\sim 1 \times 10^{20}$ Nm centered at 110 ± 50 s before the high-frequency origin time.
38. S. Kedar and T. Tanimoto (personal communication, 1993) have observed amplitude and phase anomalies of certain low-frequency spheriodal modes (${}_0S_4$, ${}_0S_6$, ${}_0S_9$, ${}_5S_3$, and ${}_1S_8$) that are consistent with the existence of a slow precursor.
39. We thank S. Kedar for pointing out the importance of the high-gain CTAO record in constraining the smoothness of the slow precursor and for useful discussions about directivity effects. We are also grateful to P. Puster for providing the synthetic seismograms used to assess the effects of mode coupling, C. Marone for insights about source mechanics, and J. Park and G. Ekstrom for helpful reviews. This research was sponsored by the National Science Foundation under grant EAR-9018690 and the National Aeronautics and Space Administration under grant NAG5-1905. P.F.I. was partially supported by grants from the Huber-Kudlich Stiftung and Sunburst Fonds.

17 March 1993; accepted 1 June 1993

(Continued from page 149)

REFERENCES AND NOTES

1. D. E. Buzzelli, *Science* **259**, 584 (1993).
2. C. K. Gunsalus, paper presented at the annual meeting of the American Association for the Advancement of Science, Chicago, IL, 6 February 1992, Symposium on Integrity and Misconduct in Science.
3. Hearings before the Subcommittee on Investigations and Oversight of the Committee on Science and Technology, U.S. House of Representatives, 97th Congress, 31 March to 1 April 1981.
4. Section 493 of the amended Public Health Service Act constitutes the Enabling Act requiring the secretary of Health and Human Services to issue regulations requiring investigation of "alleged scientific fraud which appears substantial." This language is especially significant in terms of the wide variety of misdeeds now subject to investigation and imposition of sanctions by NSF and NIH. K. D. Hansen and B. C. Hansen [*FASEB J.* **5**, 2512 (1991)], in their critical analysis of "Scientific Fraud and the Public Health Service Act," emphasized that the amendment is clear on its face but there has been a tendency by the agencies to greatly expand the authority granted.
5. The current NSF definition of misconduct in science is: (i) fabrication, falsification, plagiarism, or other serious deviation from accepted practices in proposing, carrying out, or reporting results from activities funded by NSF or (ii) retaliation of any kind against a person who reported or provided information about suspected or alleged misconduct and who has not acted in bad faith (45 C.F.R. §689).
6. R. M. Anderson, *Select Legal Provisions Regulating Scientific Misconduct in Federally Supported Research Papers* (AAAS–American Bar Assocation National Conference of Lawyers and Scientists Project on Scientific Fraud and Misconduct, Report on Workshop Number Three, American Association for the Advancement of Science, Washington, DC, 1989).
7. Testimony by H. K. Schachman before the Subcommittee on Investigations and Oversight of the Committee on Science, Space, and Technology, U.S. House of Representatives, 101st Congress, 28 June 1989.
8. Semiannual Report of the Office of Inspector General of the National Science Foundation, 1 April to 30 September 1990.
9. *Responsible Science: Ensuring the Integrity of the Research Process* (National Academy Press, Washington, DC, 1992), vol. 1.
10. Many of the cases of misconduct in science are described as plagiarism (First Annual Report of Scientific Misconduct Investigations Reviewed by Office of Scientific Integrity Review, March 1989 to December 1990, of the Public Health Service; Semiannual Report of the Office of Inspector General of the National Science Foundation, No. 6, 1 October 1991 to 31 March 1992, and No. 7, 1 April 1992 to 30 September 1992). A definition of plagiarism as misappropriation of intellectual property would suffice for adjudicating the case at Michigan State University reported by E. Marshall [*Science* **259**, 592 (1993)]. Based on the findings described by the independent panel (as reported in *Science*), the verdict of misconduct of science should have been attributed to plagiarism. There is no need to invoke the clause "a serious deviation from accepted practices."
11. In addition to the hearings in (*3*), a subcommittee of the Committee on Government Operations, House of Representatives, 100th Congress, held hearings on 11 and 12 April 1988 dealing with "Scientific Fraud and Misconduct and the Federal Response" under the chairmanship of the late Congressman Ted Weiss. On 12 April 1988, a hearing on "Fraud in NIH Grant Programs" was held by the Subcommittee on Oversight and Investigations of the Committee on Energy and Commerce, House of Representatives, 100th Congress, under the chairmanship of Congressman John D. Dingell. The Subcommittee on Human Resources and Intergovernmental Relations of the Committee on Government Operations of the U.S. House of Representatives, 100th Congress, held hearings on 29 September 1989, entitled "Federal Response to Misconduct in Science: Are Conflicts of Interest Hazardous to Our Health?" "Scientific Fraud" was the title of hearings of the Subcommittee on Oversight and Investigations of the Committee on Energy and Commerce of the U.S. House of Representatives, 101st Congress, 4 to 9 May 1989 and 30 April and 14 May 1990.
12. One might wonder whether a scientist who uses NSF funds to employ an illegal alien as a technician will be guilty of misconduct in science rather than of violating immigration and, perhaps, tax laws.
13. D. P. Hamilton, *Science* **255**, 1345 (1992).
14. Eliminating this open-ended part of the definition will reduce the burdens on governmental officials, thereby facilitating their concentration on fraud of a substantial nature. Already the staff at ORI numbers about 50 people with an annual budget of $5 million.
15. This paper was presented in part at the 6th Annual Symposium of the Protein Society, San Diego, CA, 28 July 1992, and at the Sigma Xi Forum, "Ethics, Values, and the Promise of Science," San Francisco, CA, 25 to 26 February 1993.